IEEE Access
Multidisciplinary | Rapid Review | Open Access Journal

Received July 6, 2019, accepted July 30, 2019, date of publication August 13, 2019, date of current version September 11, 2019.

Digital Object Identifier 10.1109/ACCESS.2019.2934981

Retinex-Based Laplacian Pyramid Method for Image Defogging

JINGCHUN ZHOU, (Student Member, IEEE), DEHUAN ZHANG, PEIYU ZOU, WEIDONG ZHANG, (Student Member, IEEE), AND WEISHI ZHANG

School of Information Science and Technology, Dalian Maritime University, Dalian 116026, China

Corresponding author: Weishi Zhang (teesiv@dlmu.edu.cn)

This work was supported in part by the National Natural Science Foundation of China under Grant 61702074, in part by the Liaoning Provincial Natural Science Foundation of China under Grant 20170520196, in part by the Fundamental Research Funds for the Central Universities under Grant 3132019205, and in part by the Fundamental Research Funds for the Central Universities under Grant 3132019354.

ABSTRACT To address the problem that the retinex algorithm cannot effectively enhance color and detail simultaneously, we propose a retinex-based laplacian pyramid method for image defogging. The method is implemented via MSRCR and laplacian pyramid, and it doesn't require additional hardware devices. The overall defogging process is composed of three vital parts: illumination color enhancement, detail of reflection component enhancement, and linear weighted fusion. Firstly, we add the gamma correction illumination back to reflection to achieve color enhancement. And then, the detail enhancement is achieved by the laplacian pyramid to process the reflection component. Finally, the detail enhanced image and color corrected image are used to reconstruct the clear image. Comparing with the state-of-the-art image defogging methods, the experimental results have shown that the contrast of defogged images can be effectively improved by the proposed method, and with better effects on both subjective and objective results. The contrast of images can be enhanced by the proposed method. Meanwhile, sufficient details can be preserved. Therefore, the proposed method is an effective image defogging method.

INDEX TERMS Image defogging, bilateral filter, MSRCR, Laplacian pyramid, color enhancement.

I. INTRODUCTION

Image defogging plays a crucial role, it has been applied in many areas, such as target detection, image segmentation, and visual perception. In outdoor conditions, images are collected under bad weather, including rainy, snowy, low light or foggy conditions. The contrast and visibility of images degrade due to the influence of brightness or reflection of particles. The goals of image defogging to highlight the regions of interest, enrich image color and detail information, and improve image quality [1], [2]. Therefore, research on image defogging is necessary [3]–[5]. We show a comparison between foggy images and defogged images in Figure. 1. The foggy images are shown in Figure1. (a), which directly affects the visual perception of human eyes. The defogged images by our method have richer detail information and better visual perception in Figure. (b). It can be clearly seen that the image details are blurred and with a gray layer in Figure.1 (a) compared to Figure .1 (b). The defogged images are widely applied for many scenes, such as traffic monitoring [6], remote sensing image correction [7], underwater detection [8], and medical image detection [9].

The quality of the captured image by the camera is greatly affected in the foggy, rainy, and low light conditions. Therefore, we need to obtain better visual effects and richer color and detail information by defogging methods. In the past decade, a large number of defogging methods have been proposed to deal with the degradation of the image and improve the contrast of the image. Based on different defogging principles, these mainstream methods can be classified into two categories: image restoration methods based on the physical model [10] and image defogging methods based on image enhancement [11].

The restoration methods based on physical model address the inverse process of the image degradation using the atmospheric scattering model [12], and restore the foggy image to the clear image without free-fog. Depending on the machine vision system or the type of scene, we classify the defogging methods based on physical model into five categories,

The associate editor coordinating the review of this article and approving it for publication was Yong Wang.

FIGURE 1. Instances of foggy and defogged images. The first column displays two foggy images, and the second column displays the defogging images by the proposed method.

which are based on the scene depth information, based on atmospheric light polarization, based on prior information knowledge, data hypothesis, and deep learning.

The first method is based on scene depth information. Nayar and Narasimhan [13], Narasimhan and Nayar [14], and Wang *et al.* [15] recovered the scene from two or more images by acquiring scene depth information of the same scene with different weather conditions. The scene depth information obtained by the method was complex. Therefore, the method is limited in the course of practical application. The second type of method is based on the atmospheric light polarization. Schechner *et al.* [16] achieved defogged image by the difference between the maximum and minimum polarized images of the unified scene to estimate the ambient light intensity, where the polarized image was acquired by the rotating polarizer. However, the method was highly dependent on ambient light, and the algorithm performance was poor in dense fog conditions. The third method is based on prior information knowledge. Narasimhan and Nayar [17] used scene prior information to recover defogged images. This method was not suitable for scenes with discontinuous scene depths. The fourth type of method is based on prior data. After analyzing a large number of images, Dong *et al.* [18], Nishino *et al.* [19], and He *et al.* [20] obtained the information of a scene from a single image. And the optimal method was used to solve the model parameters by constructing the cost function and constraint equation to satisfy the hypothetical conditions. The method restored a fog-degraded image to a defogged image. However, It was difficult to obtain prior knowledge when the subject color was close to the skylight. Meanwhile, the calculation process was complicated. Image defogging methods based on deep learning can be divided into two categories: the method of neural network to estimate the parameters in the atmospheric scattering model, and the method which directly outputs the defogged image by the neural network. The method based on estimating the atmospheric scattering model parameter mainly includes Cai *et al.* [21], Zhang and Patel [22] and Yang *et al.* [23], it solved the problem of setting features manually. Cai *et al.* [21], Zhang and Patel [22] and Yang *et al.* [23] proposed an end-to-end model-based CNN to estimate transmission $t(x)$ in the atmospheric degradation model, but the method cannot accurately estimate the global atmospheric light A. Li *et al.* [24], Chen *et al.* [25], Ren *et al.* [26] and Engin *et al.* [27] directly obtained the defogged image by the neural network. Li *et al.* [24] proposed AOD-Net based on a reformulation of the Koschmieder model to obtain defogged images and promoted the field of video dehazing. Chen *et al.* [25] proposed a gated context aggregation network, which solved the problem of grid artifacts. Ren *et al.* [26] obtained the defogged image by estimating the weight matrix for the processed image by the gated fusion network. Engin *et al.* [27] trained Cycle-Dehaze by feeding clean and hazy images in an unpaired manner. Although the image defogging methods based on deep learning made remarkable achievements, it has requirements of hardware devices, and it requires a large amount of training data. In summary, the restoration method based on the physical model has limited practical applications. Since it requires special physical equipment and the defogging process is complicated.

The image defogging based on image enhancement methods do not need to consider the reason for the image degradation. It has become the current mainstream method, due to the reason that it can be separated from the physical device. The goal of the image enhancement methods are used to improve contrast of image, including histogram equalization [28]–[30], smooth filter [31]–[34], and retinex enhancement [35]–[38]. Histogram equalization [28]–[30] could increase the dynamic range and improve the global contrast of the image. However, there may be some phenomena such as missing information and false contours, when the foggy density in the image is unbalanced, and the scene depth information is unknown. Histogram equalization of mean filtering [31] could enhance the image contrast, but could not bring enhanced details and remove noise effectively. In addition, a phenomenon of overexposure existed. Median filter [32] could smooth and remove noise effectively, but it may cause damage to the edges of image and blur image details when dealing with low-density noise, which was more complexed than other algorithms. Homomorphic filter [33] was used to remove low-frequency information from the foggy image. However, there were many residual components of the mist, and the local details were not prominent when the high-frequency information was retained. Unlike other filter methods, bilateral filter [34] is a nonlinear filter method. It can combine image spatial proximity and pixel similarity to achieve noise reduction and edge preservation.

Retinex [35] is a method based on constant color. In the retinex theory, single-scale retinex [36] (SSR) is the first method, which is mainly used for grayscale image enhancement, but it does not guarantee that the image is balanced

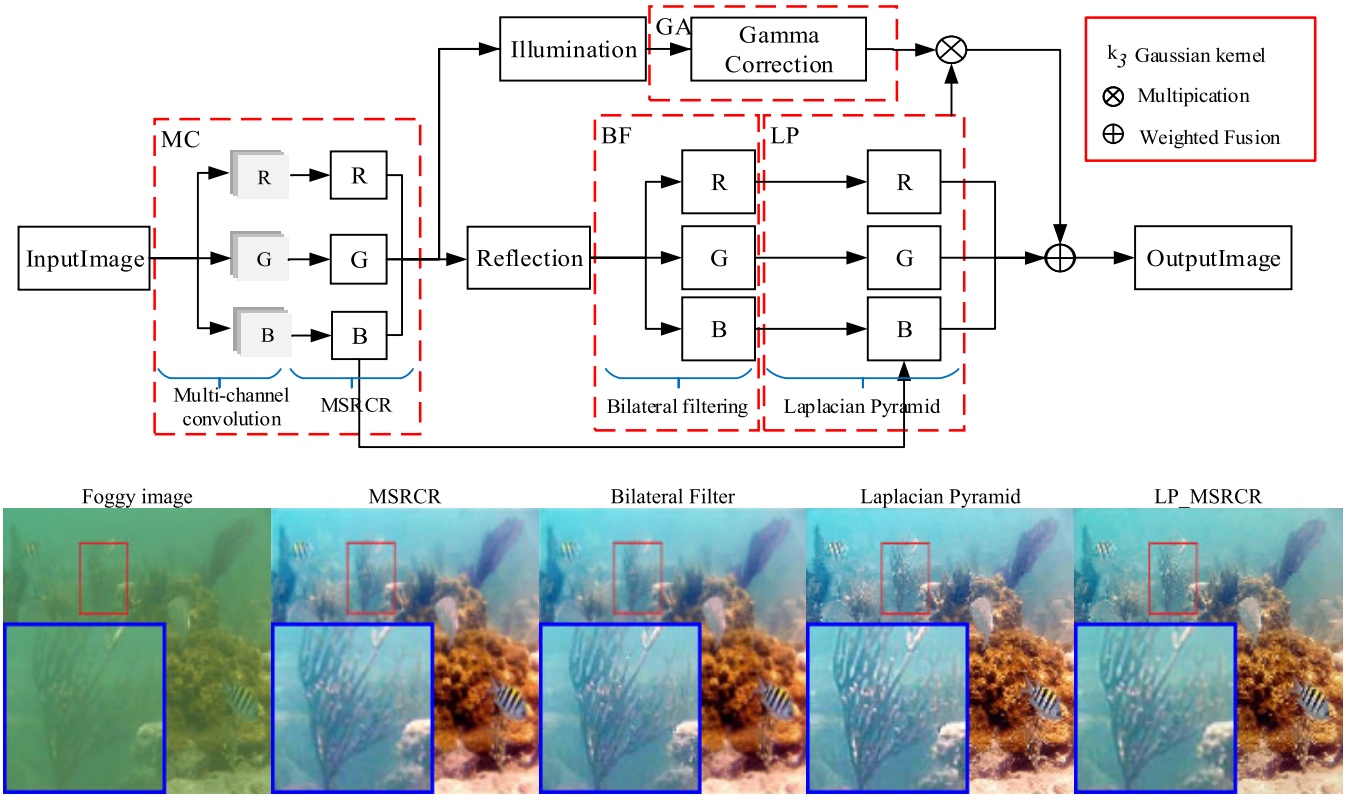

FIGURE 2. LP_MSRCR framework and amplified details of each core processes, from left to right: the foggy image,the result of the MSRCR, the result of the bilateral filter, the result of the Laplacian pyramid, and the result of the LP_MSRCR.

between detail extraction and color fidelity. Multi-scale retinex [37] (MSR) was proposed based on SSR, it achieved color image enhancement by linear weighted multiple SSR with different scales, but the algorithm may result in color distortion. To overcome the disadvantages of MSR, multi-scale retinex with color restoration [38] (MSRCR) was proposed. The MSRCR [38] introduces a color recovery factor to compensate for the color loss defects in MSR [37]. However, the enhanced image after MSRCR with halo artifacts, and it was more difficult to enhance the details of the brighter part. Elad [39] proposed a retinex algorithm based on the bilateral filter. Although the edge information was preserved, the halo artifacts were not solved completely. The MSRCR utilized by Liu *et al.* [40] effectively solved the problem of color distortion in MSR, but it couldn't achieve detail enhancement. Shen *et al.* [41] proposed a method for measuring mixed exposure weights, and the laplacian pyramid could better obtain the detail texture information of the image, and then used exposure weights to guide the completion of image enhancement. These problems of the above methods are obvious, such as color distortion, noise interference, and loss of detail in the aspect of image enhancement.

In summary, these image restoration methods based on physical model and image enhancement methods have advantages and disadvantages in the defogging fields. Due to the reason that the image enhancement method can avoid the dependence on physical devices effectively, this paper proposes an image defogging method based on retinex of laplacian pyramid (LP_MSRCR). Firstly, the method uses MSRCR to estimate the illumination. Then, Gamma correction for color enhancement is performed on the illumination, and the laplacian pyramid is used to enhance the details of the reflection. Finally, the corrected illumination is added to the reflection component, and the result is weighted with the image processed by the laplacian pyramid.

The main contributions of the proposed method include five aspects as follows:

1) To accurately estimate the illumination, we adopt a multi-scale gaussian convolution kernel to convolve each channel. The illumination is estimated from convolving three gaussian kernels with different scales to extract rich feature.
2) MSRCR is used to decompose the convolved image to obtain illumination and reflection. Color natural performance is ensured by performing gamma correction on the illumination and compensation on the enhancement result.
3) Considering the reflection contains a large amount of high-frequency information such as local feature details and noise. We perform a bilateral filter on reflection, which can suppress noise interference and preserve edge effectively.

4) For obtaining rich edge detail information. We obtain edge detail from the enhanced image of MSRCR. The edge detail information and bilateral filtered image are used as input of Laplacian pyramid.
5) In order to preserve the natural property of the defogging image. The illumination after color correction is added back to reflection after detail enhanced. The result is linear weighted with the reflection image to reconstruct the final fog-free image.

The rest of this paper is organized as follows. This paper presents details of our proposed method, includes detail enhancement, color enhancement, and liner weighted fusion in Section II. The detailed experimental results and analysis are presented in Section III, which includs various processes, subjective and objective comparisons. Finally, we summarize the conclusions and future exploration work in Section IV.

II. PROPOSED ENHANCEMENT METHOD

In this section, we propose a retinex-based laplacian pyramid method for image defogging. Figure. 2 shows a framework of the method and an amplified view of the details. The whole process of the method is divided into four parts, including estimate the illumination by the multi-scale convolution MSRCR, denoise the reflection by the bilateral filter, enhance the detail of reflection component by the Laplacian pyramid, and color enhancement of illumination by gamma correction. The details of the four core processes are amplified. In Figure.2, from left to right, the foggy image, the images are obtained by MSRCR, bilateral filter, laplacian pyramid, and LP_MSRCR. At the beginning and the end of the image processing, it is clearly shown that LP_MSRCR algorithm can effectively enhance the image details and preserve naturalness.

1) To extract more detail information, the original image is subjected to multi-scale convolution [46]. Thereby each channel from *RGB* color space of the original image is convoluted by three gaussian kernels with different scales. In our work, the size of the convolution kernel is 3*3, which is set to be 3.
2) The image contrast is enhanced by the MSRCR. From the perspective of quantification [40], mean value and mean square error are introduced to limit the stretching degree of image contrast. Color equalization is achieved by controlling the dynamic parameters of the image to avoid color distortion.
3) To achieve color enhancement, the MSRCR is used to decompose the illumination and reflection of the image. Improved gamma correction is applied to the illumination image [42]. The correction parameter is adaptively calculated by judging the mean value of the image pixels, and the illumination compensation is performed. Finally, color consistency is guaranteed by previous operations.
4) The reflection component contains much high-frequency information, such as edge details and noises. The MSRCR will amplify the noise during the image enhancement. Therefore, the reflection image is performed by the bilateral filter [39], which can effectively remove noise and preserve edge details simultaneously.
5) In order to achieve the detail enhancement, the image after the bilateral filter and the enhanced reflection image of MSRCR are jointly used as the input image of the laplacian Pyramid.
6) To preserve naturalness, the corrected illumination is added back to the reflection [43], [44], and the color corrected image is linear weighted fuse with the reflection image to reconstruct the clear image. It can preserve color natural performance.

The framework of the LP_MSRCR method pseudo-code is as follows:

Algorithm 1 Framework of the LP_MSRCR Algorithm

(1) Input: Foggy image $I(x, y)$
(2) Estimate the illumination $L(x, y)$ using (2) and (3) based on MSRCR.
(4) Estimate the reflection $R(x, y)$ using (4) and (8) based on MSRCR.
(5) Iteration: iterate on $x = 1, 2, \ldots, N$, $y = 1, 2, \ldots, M$
  (a) Update $Bf(x, y)$ using (15) based on bilateral filter.
  (b) Update $LL(x, y)$ using (23) based on laplacian pyramid.
  (c) Update $Ga(x, y)$ using (31) based on gamma correction.
  (d) Update S' using (32) based on reconstructing the color enhanced image.
  (e) Update $Result(x, y)$ using (33)(34)(35) based on liner weighted fusion.
(6) Output: $Result(x, y)$

A. DETAIL ENHANCEMENT

1) CONTRAST ENHANCEMENT OF MSRCR

In order to achieve dynamic balance, edge enhancement and color constant, MSRCR [10] method based on retinex is adopted. The retinex [36] is an image enhancement method, which is based on the color constant theory. The retinex is expressed that the product of illumination and reflection component as follows:

$$S(x, y) = L(x, y) \cdot R(x, y) \tag{1}$$

where $S(x, y)$ is an observed image, $L(x, y)$ is the illumination, which corresponds to the low-frequency information of the image. $R(x, y)$ is the reflection component, which corresponds to the information of the image high frequency (e.g., texture and edge information) and reflects the intrinsic nature of the image. The aim of the retinex is estimated the illumination and then remove the illumination to obtain the reflection component.

The SSR cannot achieve dynamic range compression and contrast enhancement of the image simultaneously. Therefore, the MSR [37] was proposed. It can achieve dynamic range compression and color fidelity by linear weighted

fusion SSR of different scales.

$$L_i(x, y) = S_i(x, y) * G_k(x, y) \tag{2}$$

$$G_k(x, y) = \frac{1}{2\pi\sigma^2} e^{-(\frac{x^2+y^2}{2\sigma^2})} \tag{3}$$

$$\begin{aligned} R_{MSR_i}(x, y) &= \sum_{n=1}^{k} \omega_k R_{SSR_i} \\ &= \sum_{n=1}^{k} \omega_k \{\log S_i(x, y) - \log[L_i(x, y)]\} \end{aligned} \tag{4}$$

where i is one of the channels from R, G, B color space in the image, k is the number of scales, the illumination $L_i(x, y)$ can be approximated from $S_i(x, y)$ by a gaussian filter convolution, $R_{MSRi}(x, y)$ is the processing result in the i^{th} channel, $G_k(x, y)$ is a multi-scale gaussian function, and ω_k is the weighted factor. Considering the time complexity and enhanced effect, the scale value k is usually set to be 3, which is divided into three scales of low, medium and high, with low scale is $\lambda < 5$, the medium scale is $5 \leq \lambda < 10$, and high scale is $\lambda \geq 10$.

Due to the color distortion of MSR, MSRCR introduces a color recovery factor to avoid local contrast enhancement and color distortion. Therefore, this paper adopts improved MSRCR [47]. We proceed with the GIMP of image enhancement algorithm from the perspective of quantification. In the process of adjusting the color distortion, the mean and the variance are used to obtain the maximum and minimum pixels values on each channel, and a dynamic parameter is used to make the color fidelity more adaptive to various scene images. The calculative process as follows:

$$\begin{aligned} &R_{MSRCR_i}(x, y) \\ &\quad = C_i(x, y) R_{MSR_i}(x, y) \end{aligned} \tag{5}$$

$$\begin{aligned} &Min \\ &\quad = Mean(R_{MSR_i}) - Dynamic \cdot Var(R_{MSR_i}) \end{aligned} \tag{6}$$

$$\begin{aligned} &Max \\ &\quad = Mean(R_{MSR_i}) + Dynamic \cdot Var(R_{MSR_i}) \end{aligned} \tag{7}$$

$$\begin{aligned} &R_{MSRCR_i}(x, y) \\ &\quad = \sum\nolimits_i 255 \\ &\qquad \cdot \frac{\{R_{MSR_i} - Mean(R_{MSR_i}) + Dynamic \cdot Var(R_{MSR_i})\}}{2 \cdot Dynamic \cdot Var(R_{MSR_i})} \end{aligned} \tag{8}$$

where the *Dynamic* is the dynamic factor (usually *Dynamic* = 2), *Mean* and *Var* are the mean and variance of pixel values, respectively.

For ensuring the range of pixel values in [0, 255], the overflow judgment is added. It can be defined as follows:

$$R_{MSRCR_i}(x, y) \begin{cases} 0 & R_{MSRCR_i}(x, y) < 0 \\ R_{MSRCR_i}(x, y) & 0 \leq R_{MSRCR_i}(x, y) \leq 255 \\ 255 & R_{MSRCR_i}(x, y) > 255 \end{cases} \tag{9}$$

2) NOISE REDUCTION OF BILATERAL FILTERING

The goal of maintaining edges and filtering noise is achieved by the bilateral filter [39], which requires the use of spatial proximity and nonlinear combination of luminance similarities to determine the weighted coefficients. The algorithm not only solves the noise amplification but also extracts the detail features and edge information for subsequent operation. The specific definition is expressed as follows:

$$h(x) = \frac{1}{k_r} \int_{-\infty}^{+\infty} \int_{-\infty}^{+\infty} f(\xi) s(f(\xi), f(x)) d\xi \tag{10}$$

$$h(x) = \frac{1}{k_d} \int_{-\infty}^{+\infty} \int_{-\infty}^{+\infty} f(\xi) c(\xi, x) d\xi \tag{11}$$

where $s(f(\xi), f(x))$ is the brightness similarity, $k_r(x)$ and $k_d(x)$ are normalization coefficients, and $c(\xi, x)$ is the euclidean distance between ξ and x.

The bilateral filter can be expressed as an image pixel spatial position and luminance similarity to calculate the weight between adjacent pixels. The transfer function is expressed as:

$$Bf_i(x, y) = h(x) = \frac{1}{k(x)} \int_{-\infty}^{+\infty} \int_{-\infty}^{+\infty} f(\xi) c(\xi, x) s(f(\xi), f(x)) d\xi \tag{12}$$

where $Bf_i(x, y)$ is the input function, and $Bf_i'(x, y)$ is the output function. Then the discrete form of the bilateral filter is defined as:

$$Bf_i'(x, y) = \sum_{m=-q}^{q} \sum_{n=-q}^{q} A[m, n, x, y] Bf_i[x - m, y - n] \tag{13}$$

where $A[m, n, i, j]$ is a gaussian function, which is described as:

$$A[m, n, x, y] = \frac{exp(-\frac{m^2+n^2}{2\sigma_d^2} - \frac{(R[x,y]-R[x-m,y-n])^2}{2\sigma_r^2})}{C[x, y]} \tag{14}$$

where (x, y) is the current pixel, (m, n) is the neighboring pixel, $R(x, y)$ is the corresponding pixel value, σ_d is the spatial domain filter standard deviation, and σ_r is the value domain filter standard deviation.

The detailed derivation process of the bilateral filter is shown in formula (13) and (14).

$$Bf_i = B\_filter(I, G, Sigma\_d, Sigma\_r, filterRadius) \tag{15}$$

The bilateral filter formula is (15), where i is the corresponding image channel, I is the input image, G denotes the guided image after I normalization, *sigma_d* is the kernel parameter of time domain in spatial domain, *sigma_r* is the intensity variation range of kernel parameter, and *filterRadius* is the radius of the bilateral filter. It can be known from I that the original image is firstly decomposed into three channels, and then the R, G, and B channels are filtered. Note that the detailed solution is reference [39].

$$Bf_R = B\_filter(R, G_R, Sigma\_d, Sigma\_r, filterRadius) \tag{16}$$

$$Bf_G = B\_filter(G, G_G, Sigma\_d, Sigma\_r, filterRadius) \tag{17}$$

$$Bf_B = B\_filter(B, G_B, Sigma\_d, Sigma\_r, filterRadius) \tag{18}$$

where *sigma_d*=5, *sigma_r*=0.03 and *filterRadius*=15, they are determined by large amount of experiments.

3) FEATURE EXTRACTION OF LAPLACIAN PYRAMID

To solve the problem of losing portion edge detail of the image after the bilateral filter, and to obtain the detailed feature information of different decomposition layers, the following methods can be adopted. First, the enhanced image of MSRCR is decomposed into different spatial frequency bands by laplacian pyramid. More edge information and detail information are extracted by processing separately on each spatial frequency layer. The above information is weighted fused with the bilateral filtered image to enhance the detail of image.

The laplacian pyramid was proposed by Burt and Adelson [45] and evolved from gaussian pyramid. First, the image is decomposed by gaussian pyramid, assuming the original image is G and G_0 is the 0^{th} layer of the gaussian pyramid. Gaussian low-pass filtering and interlaced subsampling are performed on the original image to obtain the first layer of the gaussian pyramid. Then the low-pass filtering and downsampling of the first layer image are performed to obtain the second layer of the gaussian pyramid. Repeat the above process, a gaussian pyramid is constructed. During the process, the construction of the gaussian pyramid is given as:

$$G_L = \sum_{m=-2}^{2}\sum_{n=-2}^{2} \omega(m,n) G_{L-1}(2x+m, 2y+n), \quad (1 \le L \le N, 0 \le x \le R_L, 0 \le y \le C_L) \tag{19}$$

where N is the number of layer in the gaussian pyramid, R_L and C_L are the numbers of row and column of the L^{th} layer in the gaussian pyramid, respectively, and $\omega(m, n)$ is a two-dimensional low-pass filter. Gaussian pyramid consists of $G_0, G_1 \ldots G_N$, where G_0 is the bottom of the pyramid.

The laplacian pyramid can be obtained by finding the difference between every two layers of the image in the gaussian pyramid. The interpolation method is performed by the k^{th} layer image G_k and G_k is enlarged to G_k^*, so that the size of G_k is the same as the size of G_{k-1}, and the specific equation is expressed as:

$$G_k^*(x,y) = 4\sum_{m=-2}^{2}\sum_{n=-2}^{2} \omega(m,n) G_k'\left(\frac{x+m}{2}, \frac{y+n}{2}\right), \quad (1 \le L \le N, 0 \le x \le R_{k-1}, 0 \le y \le C_{k-1}) \tag{20}$$

where G_k is the k^{th} layer of the pyramid, G_k^* is the expanded image of G_k, the image G_{k-1} of the $k-1^{th}$ layer is expressed by:

$$LP_{k-l} = G_{k-l} - G_k^* \tag{21}$$

formula (21) generates the $k-1^{th}$ layer of the Laplacian pyramid. Since G_k is low-pass filtering and downsampling by G_{k-1}, the details of G_k are significantly less than G_{k-1}. Therefore, the details of G_k^* are obtained by G_k interpolation, which are still less than G_{k-1}. LP_{k-1} is the differentials between G_k^* and G_{k-1}, it not only reflects the differential between the different layers of gaussian pyramid G_k and G_{k-1} but also includes the high-frequency information lost during G_{k-1} re-blurring and downsampling. The laplacian pyramid is defined as:

$$\begin{cases} LP_k = G_k - G_k^*, & (0 \le k \le N) \\ LP_N = G_N, & (k = N) \end{cases} \tag{22}$$

where N is the top layer number of the laplacian pyramid, LP_L is the L^{th} layer image of the laplacian pyramid, and $LP_0, LP_1 \ldots, LP_L \ldots, LP_N$ constitute the laplacian pyramid.

The laplacian pyramid formula is defined as:

$$LL_i = LLS(Bf_i, R_{MSRCR_i}, Layers, Sigma_1, Radius_1, Sigma_2, Radius_2, \lambda) \tag{23}$$

where Bf_i is the bilateral filter image, R_{MSRCR_i} is the enhancement image of MSRCR, *Layers* is the number of layer in the pyramid, $Sigma_1$ is the scale of the first pyramid, $Radius_1$ is the radius of the first pyramid, $Sigma_2$ is the scale of the second pyramid, $Radius_2$ is the radius of the second pyramid, and λ is the detail weight coefficient. The expression after the laplacian pyramid for R_{MSRCR_i} using the each channel from *RGB*color space is as defined in formula (24)(25)(26):

$$LL_R = LLS(Bf_R, R_{MSRCR_R}, Layers, Sigma_1, Radius_1, Sigma_2, Radius_2, \lambda) \tag{24}$$

$$LL_G = LLS(Bf_G, R_{MSRCR_G}, Layers, Sigma_1, Radius_1, Sigma_2, Radius_2, \lambda) \tag{25}$$

$$LL_B = LLS(Bf_B, R_{MSRCR_B}, Layers, Sigma_1, Radius_1, Sigma_2, Radius_2, \lambda) \tag{26}$$

The selection of the parameters is based on a large number of experimental results, such as $Layers = 3$, $Sigma_1 = 5$, $Radius_1 = 5$, $Sigma_2 = 10$, $Radius_2 = 8$ and $\lambda = 2.5$.

The improved laplacian pyramid firstly downsamples the *Layer*, *Layers* of two different scale gaussian pyramids of R_{MSRCR_i} and then obtains two *Layer* gaussian pyramids to differentiate and then obtains the laplacian pyramid detail image. Then, the preset detail weight coefficient $\lambda(\lambda > 1)$ is added to the bilateral filter image to obtain a detailed image of the laplacian pyramid.

$$LL_i(x,y) = \lambda \cdot LP_{Layers_i} + Bf_i \tag{27}$$

B. COLOR ENHANCEMENT

The MSRCR [38] can enhance the contrast and the details of the image effectively. The illumination is directly removed, it shows an over-enhancement phenomenon to some extent. Therefore, we use the gamma correction to compensate for the image of the illumination. Adding the corrected illumination back to the reflected component is a complementary

process that ensures the enhanced image with better natural properties [43], [44].

The quality of each image is different in the practical application process. The classical gamma correction algorithm [42] redistributes pixel values by fixed parameters in the global range. Parameters of setting manually are difficult to improve the quality of each image due to the correction parameters for each image are different. Therefore, the parameter γ should be adaptively changed by the change in the pixel value. The classical gamma correction is defined as:

$$L' = W(\frac{L}{W})^{\frac{1}{\gamma}} \tag{28}$$

where r is an adjustable parameter, L' is the corrected pixel value, L is the current pixel value, and W is the maximum pixel value in an 8-bit image (usually set to be 255).

In view of the above problem, a fast gamma transform algorithm is proposed to avoid the defects of manually configurable fixed certain parameters, when r<1 the mean value of the image pixel values is in [0, 127]. The image pixels are located in the low pixel value area, at which the dynamic range is expanded, the contrast of the image is enhanced, and the pixel value of the overall image is increased. In the image, the average pixel values is in [127, 255] when r>1. The image pixel is in the high pixel value area, at which the dynamic range is expanded, the contrast of the image is enhanced, and the pixel value of the overall image is reduced.

Firstly, we obtain the image pixel value, then obtain the average of the illumination pixel value. Finally, determine the value of the parameter r by the ratio of N.

$$sum = m \cdot n \cdot p \tag{29}$$

$$\gamma = \frac{\sum_{x=1}^{m}\sum_{y=1}^{n}\sum_{z=1}^{p} L(x, y, z)}{sum \cdot N} \tag{30}$$

$$Ga_i = L_i'(x, y) = c[L_i(x, y)]^{\gamma} \tag{31}$$

where r is the correction parameter, $L_i'(x, y)$ is the channel of the illumination image, *sum* is the total number of pixels in the image L, m and n are the row and column of the illumination image, p is the number of channels of the illumination image, $p=3$ is the color image, $p=1$ is the gray image, N is the threshold for judging the brightness of the image(usually set N is 127), and c is a constant.

For maintaining the color naturalness and fidelity of defogging image, the corrected illumination image is added to the reflected component image. The color corrected image is expressed as:

$$S_i'(x, y) = Ga_i(x, y) \cdot LL_i(x, y) \tag{32}$$

where S_i' denotes the color corrected image.

C. LINER WEIGHTED FUSION

The linear weighted fusion is organized as follows:

Step 1: According to II. A 1), we can obtains R_{MSRCR_R}, R_{MSRCR_G} and R_{MSRCR_B} that are enhanced *R, G,* and *B* channels by MSRCR.

Step 2: According to II. A 2), we can obtains Bf_R, Bf_G and Bf_B that are denoised *R, G,* and *B* channels by the bilateral filter.

Step 3: In term of II. A 3), we can obtains LL_R, LL_G, and LL_B that are detailed each channel from *RGB* color space by laplacian pyramid.

Step 4: According to II. B, we can obtains Ga_R, Ga_G, and Ga_B that are corrected *R, G,* and *B* channels of the illumination by Gamma correction. Adding the corrected illumination of the color corrected images back to the reflection component, S_R', S_G' and S_B' are obtained.

According to Step3 and Step4, the detail enhancement image and the color corrected image are obtained, and then each channel form *RGB* color space is linearly weighted fusion. The equation is concluded as:

$$Result_R(x, y) = \alpha \cdot LL_R(x, y) + (1 - \alpha) \cdot S_R'(x, y) \tag{33}$$

$$Result_G(x, y) = \alpha \cdot LL_G(x, y) + (1 - \alpha) \cdot S_G'(x, y) \tag{34}$$

$$Result_B(x, y) = \alpha \cdot LL_B(x, y) + (1 - \alpha) \cdot S_B'(x, y) \tag{35}$$

where $Result_R(x, y)$, $Result_G(x, y)$, and $Result_B(x, y)$ represents the enhanced images of *R*, *G*, and *B* channels, α is the weight coefficient and set $\alpha \in (0, 1)$.

III. RESULTS AND DISCUSSION

A. MULTI-SCALE CONVOLUTION PROCESS

In this paper, the multi-scale convolution of the LP_MSRCR is used to estimate the illumination of the image, which directly affects the extraction of the image reflection component. The single-scale edge feature extraction algorithm cannot obtain edge and detail information at different scales when the illumination is estimated. Therefore, multi-scale convolution kernels are used to obtain more detail feature estimate of the illumination and reflection component.

Figure. 3 shows the result of the image of the illumination and reflection component under different smoothing weighted factor σ. Considering the time complexity and the effect of the experiment, this paper chooses to use the three-layer convolution to extract the features with different scales. As *R* changes from a low-scale $\sigma = 5$ to a high-scale $\sigma = 20$, the edge details of the illumination and reflection component are reduced gradually, but the color of the reflection component is more abundant. Single-scale feature extraction is difficult to obtain edge feature information and texture detail information at different scales. Therefore, multi-scale convolution is used to estimate the illumination. The convolution smoothing weighted factor σ_f of different scales are used to estimate the illumination, where $\sigma_f < \sigma_{f+1}, f = 1, 2, ..., k$ and k is the number of convolution filters. The k is set to be 3, $\sigma_{f+1} = 2\sigma_f$ in this paper, the three smoothing weighted factors at multi-scale are $\sigma_1 = 5, \sigma_2 = 10, \sigma_3 = 20$, respectively. Through the experiment, the detail information of illumination is not obvious when $\sigma_f > 20$. Therefore, the average

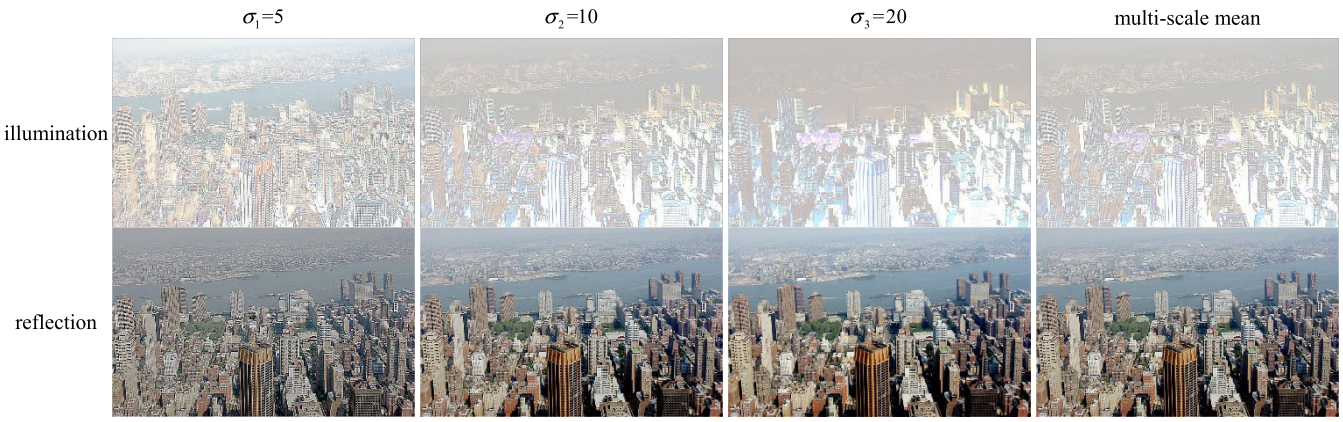

FIGURE 3. Image illumination and reflection component of smooth weighted factors at different scales. From left to right: the first column is the illumination and the reflection component image of $\sigma_1 = 5$, the second column $\sigma_2 = 10$, the third column $\sigma_3 = 20$, the fourth column is the illumination and the reflection component image after multi-scale mean.

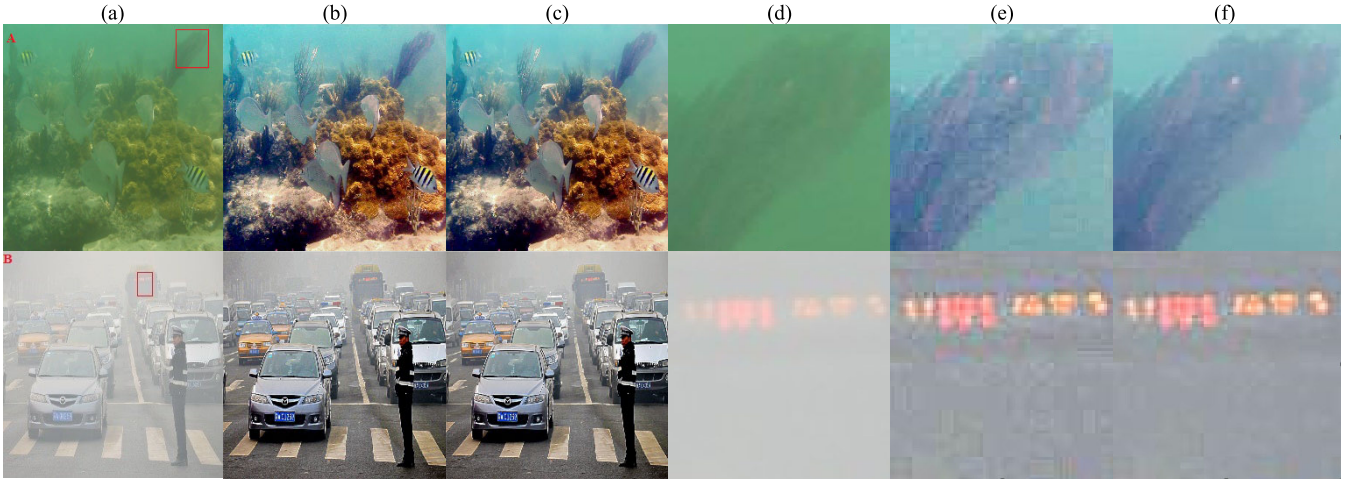

FIGURE 4. (a) The foggy image. (b) the image of the removal BF (Bilateral Filter). (c) the result by the LP_MSRCR. (d) the patch from the foggy image. (e) the patch from the images by removal BF. (f) the patch from the images by LP_MSRCR.

of the extracted edge feature information under three different scales to estimate the illumination. The reflection component is obtained by equation (14).

B. BILATERAL FILTER NOISE PROCESS

In order to verify the effectiveness of each processing step of the LP_MSRCR, it will be divided into four sections. As shown in Figure.2, MC represents Multi-channel convolution and MSRCR enhancement, BF represents Bilateral Filtering processing, LP represents laplacian pyramid processing, GA represents Gamma Correction processing.

Due to the retinex algorithm is used to achieve image detail enhancement, the stretch of the darker areas of the image is larger than the brighter areas. During image contrast enhancement, noises were amplified. Therefore, it is necessary to remove the noise of the enhanced image. The reflection component image contains much high-frequency information such as edge detail and noise, thereby the bilateral filtering process on the reflection component image can effectively eliminate noise. Therefore, the process of the reflection component image can eliminate noise effectively. To verify the effect of the bilateral filter (BF), we compare BF removal with the enhanced effect on the image of LP_MSRCR.

These images are shown in Figure. 4, the original images of the A and B, and defogging results by LP_MSRCR, the images are acquired by removal BF, the local amplification result of the red rectangle of the foggy images, defogging images are acquired by LP_MSRCR, and removal BF. Compared with the original image, the image contrast and the image detail are enhanced by LP_MSRCR, and the images are acquired by removal BF. By comparing with the image detail, it is obvious that there is more noise of the purple coral in the A scene and the front windshield of the bus in the B scene after BF removal.

C. LAPLACIAN PYRAMID DETAIL PROCESS

The core of the image enhancement is the detail enhancement, and the reflection component contains the local edge

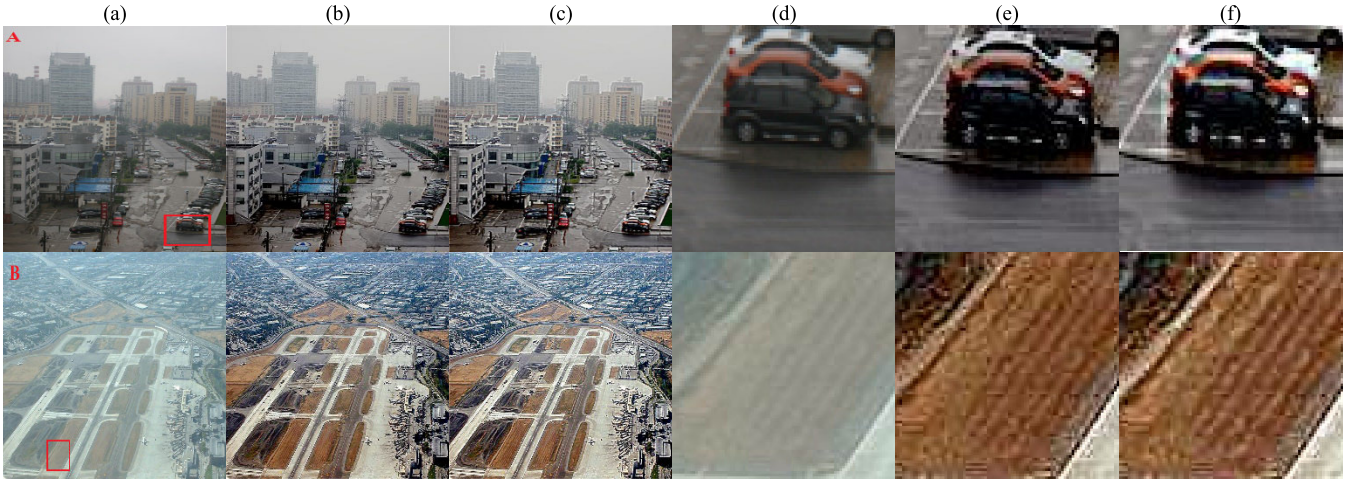

FIGURE 5. (a) The foggy image. (b) the result image by removal LP. (c) the result image by LP_MSRCR. (d) the patch from the foggy image. (e) the patch from the image by removal LP(Laplacian pyramid). (f) the patch from the image by LP_MSRCR.

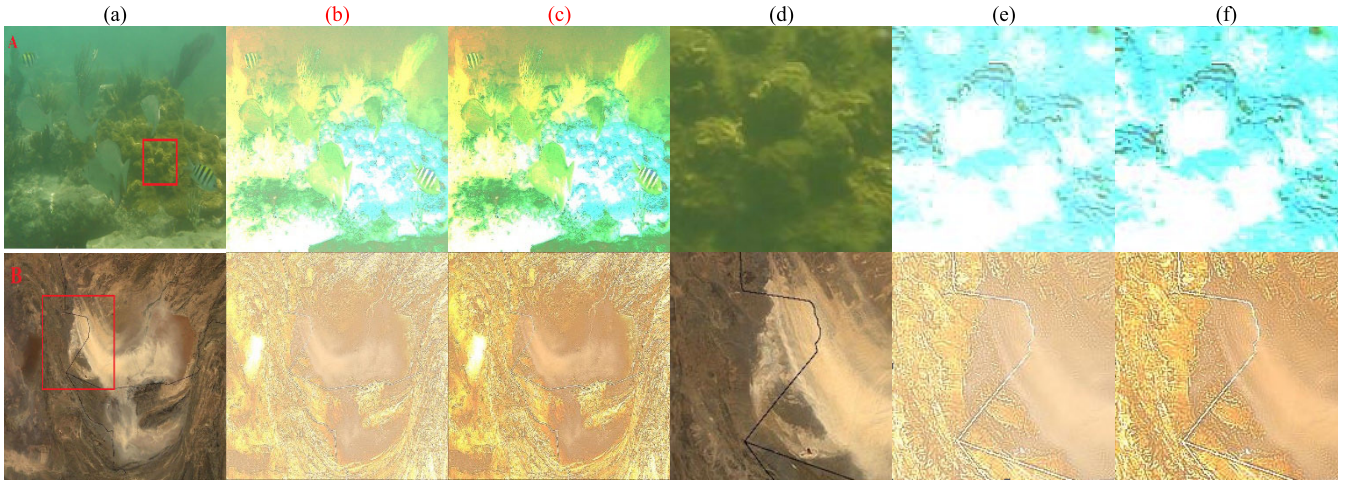

FIGURE 6. (a) The foggy image. (b) the result image by removal GA. (c) the defogging image by LP_MSRCR. (d) the patch from the foggy image. (e) the patch from the image by removal GA. (f) the patch from the image by LP_MSRCR.

information and details of the image. Because of the bilateral filter denoising will cause partial edge information loss. Therefore, the LP_MSRCR obtains the edge information from the image by MSRCR. Meanwhile, the bilateral filter image is served as the laplacian pyramid input image. This operation not only achieves image smooth and denoising but also obtains edge and detail information.

The images are shown in Figure.5, the original images of the A and B, and results by LP_MSRCR, the images are acquired by removal BF, the local amplification results in the red rectangle of the original images, LP_MSRCR, and removal LP. The contrast and detail of the image by LP_MSRCR are superior to the original image, and the images are acquired by removal LP, the edge texture details of the orange car in the A scene and the runway texture in the B scene can be clearly observed, it shows that the LP_MSRCR is better than the removal LP. In general, it can be verified that the laplacian pyramid can effectively improve the image detail information.

D. GAMMA CORRECTION PROCESS

The MSRCR is used to estimate the illumination, but directly removing the illumination will have an over-enhancement. For addressing the problem, we add the corrected illumination back to the reflection component, which realizes the illumination compensation and ensures that the enhanced image with better natural properties. To ensure the color constant of the image enhancement and compensate for the color distortion caused by the image contrast enhancement of the local field. The gamma algorithm is used to correct image brightness. In this way, image contrast is enhanced, and image edge detail information is highlighted.

These images are shown in Figure.6, the foggy image of the A and B scenes, the image processed by LP_MSRCR, the result of the removal GA, the detail image of the original image, the detail image by LP_MSRCR, and the detail image by the removed GA. The overall contrast of the images processed by LP_MSRCR and removal GA is superior to the foggy image. By comparing the detail image by the

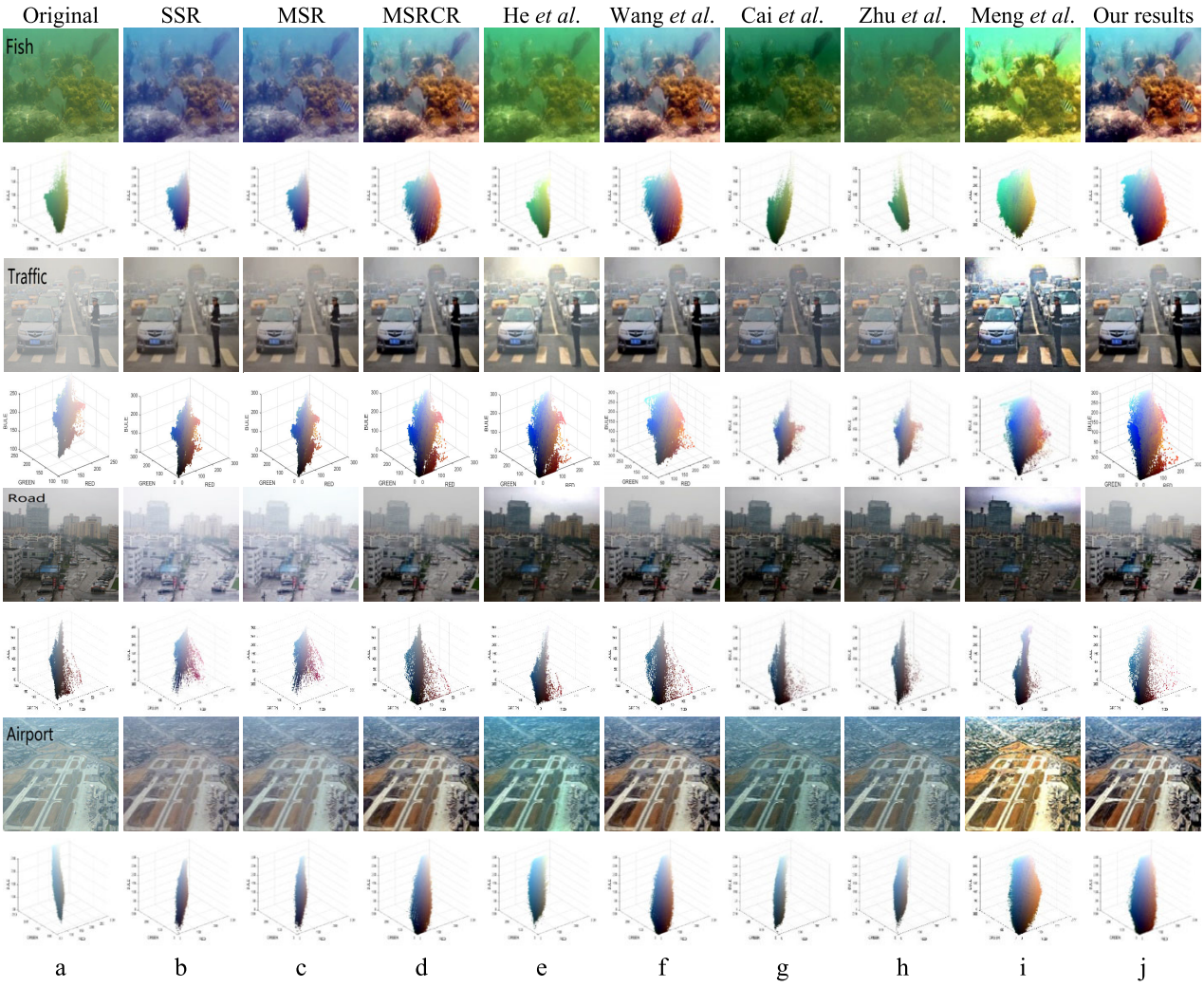

FIGURE 7. Comparisons of images of various defogging algorithm and their 3D RGB color model. (a)Input foggy images. (b)SSR results. (c) MSR results. (d) MSRCR results. (e) He *et al.* [10]. (f) Wang *et al.* [10]. (g) Cai *et al.* [21]. (h) Zhu *et al.* [49]. (i) Meng *et al.* [50]. (j) our results.

LP_MSRCR and the image of removal GA in two scenarios, the coral texture details in the A scene and the terrain regions in the B scene can be observed in the LP_MSRCR detail image. That is to say, the edge details by the LP_MSRCR are more obvious. The comparison and analysis of experiment shows that the gamma correction can improve the image details effectively.

E. SUBJECTIVE COMPARISON WITH CLASSICAL AND STATE-OF-THE-ART METHODS

In this paper, the LP_MSRCR based on retinex of laplacian pyramid is proposed. The core of LP_MSRCR is to solve the problem that image enhancement cannot retain image color and detail information simultaneously. We analyzed the subjective results of the LP_MSRCR and selected four different scene images from the common datasets. The foggy images contain fish, traffic, road, and airport. The defogging results and 3D color model images are shown in Figure.7.

We compare the performance of the LP_MSRCR with various classical image defogging methods and state-of-the-art methods. Traditional methods include SSR [36], MSR [37], and MSRCR [38]. Five state-of-the-art methods include He *et al.* [20], Wang *et al.* [10], Cai *et al.* [21], Zhu *et al.* [49], and Meng *et al.* [50]. The comparative analysis with the above methods proves the superiority of the LP_MSRCR.

Figure.7 shows the result images and 3D color model of the images using various defogging methods under different foggy scenarios. The effects of the defogging images are shown in Figure.7 (b-j). In addition, these methods can enhance dark regions, improve global contrast, and preserve local detail information. Figure.7 (b) and (c) are the results of the defogging images by SSR [36] and MSR [37], which haven't sufficiently sharpened of edge. The details of the highlighted area have not been improved.

The details of the highlighted area have not been improved, so the results appear color casts, such as the purple image

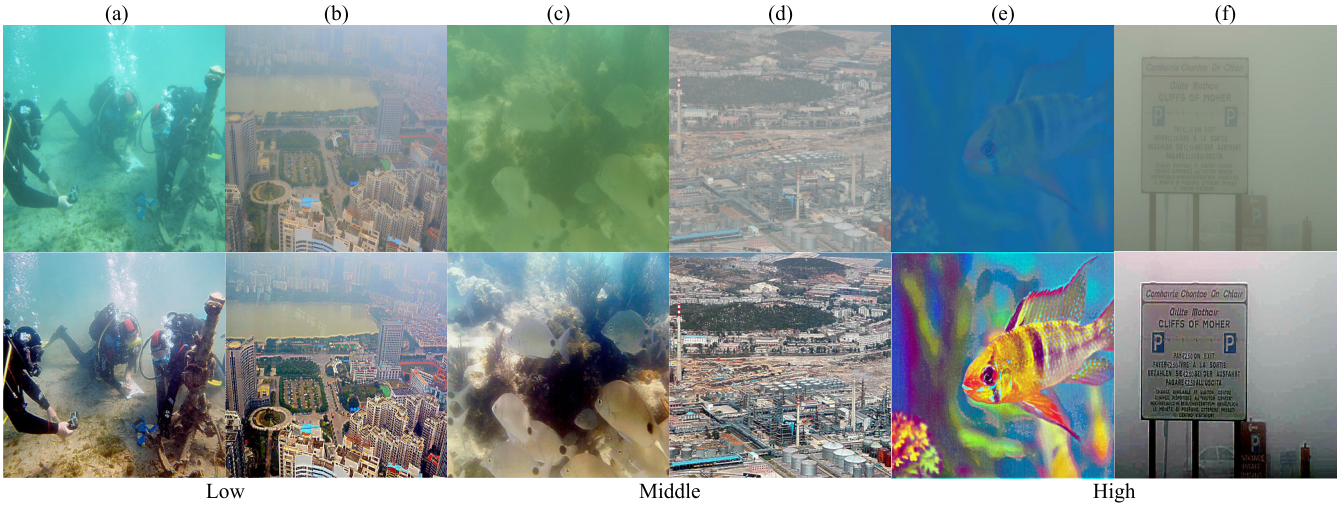

FIGURE 8. From up to down: the original images and the defogged images are obtained by LP_MSRCR operation. (a) and (b) are obtained in low concentration scenes; (c) and (d) are obtained in middle concentration scenes; (e) and (f) are obtained in high concentration scenes.

of the fish image, the white phenomenon of the road and airport image. The images which acquired by He *et al*. [20], and Cai *et al*. [21] are appeared in Figure.7 (e) and (g). The halo artifact of the defogging image is obvious, besides color cast. Such as the color of the Fish image appears dark green, the halo artifact appears in the distant image of the Traffic image, the color of the sky in the Road image is distorted. Figure.7 (h) shows the result of defogging by Zhu *et al*. [49]. It is clear that the effect of the defogging image is poor and overall slightly green. The detail information of the defogging image is lost. Figure.7 (i) shows the result of defogging Meng *et al*. [50]. It can be seen that this method has halo artifacts and overexposure. Although this method can enhance the contrast of the image, it is difficult to preserve image naturalness. Figure.7 (d), (f) and (j) are fog-free images by MSRCR [38], Wang *et al*. [10], and our method. Obviously, these methods achieved image defogging, effectively suppress halo artifact, meanwhile preserving color. However, Wang *et al*. [10] method cannot preserve the color naturalness. Figure.7 (j) is the result of the defogging image by the proposed method. Our proposed method can achieve color enhancement and detail information enhancement by analyzing the 3D color model. The proposed method can obtain a clear and natural defogging image, and it outperforms other methods.

In figure 7, it is obvious that our method can effectively remove fog. However, compared with the effect image, the defogging effect in the middle part of the image is better, but the defogging effect around the images is not satisfying. The reasons are concluded as follow:

In the close scene, the scene contains rich colors and details. The multi-scale retinex with color restoration can enhance color. At the same time, it can effectively improve the contrast of the image and enriche global detail. Because Laplacian has the advantages of extracting global contour information and local detail texture, the Laplacian is adopted for enhancing local detail, which can effectively highlight detailed features. Therefore, our method has a quite satisfying enhancement effect in the close scene.

In the far scene, since the sky area is highly similar to the thick fog, compared with the enhancement effect of the close scene, the enhancement effect of the far scene is not satisfactory. Based on the above problems, our method uses the Retinex method to blend with the Laplacian method. For global information, it needs to obtain rich color and detail information in the process of image defogging.

In this paper, the thick fog images under different scenes are selected, and after a lot of experimental verification, the method shows a good enhancement effect under a particular scene or a specific area.

To verify the concentration of the fog affecting the accuracy of the algorithm, we choose six images in three levels of concentration the fog, include low, mid, and high concentration. From up to down, the first row shows the original images, the second row shows the result images by LP_MSRCR. The three levels of concentration of the fog images are selected as the test sample, the defogged result images, as shown in the second row of Figure. 8. In the second row, we can clearly see that the defogged image has better visual effects and sharpness by our method in different foggy environments.

F. OBJECTIVE COMPARISON

1) OBJECTIVE METRICS

In order to ensure fair evaluation, we objectively analyze the experimental results of the classical methods, state-of-the-art defogging methods, and our method with different scenarios. The three most widely used objective evaluation indicators: average gradient (*AG*) [51], information entropy (*IE*) [52] and edge gradient (*EG*) [46].

TABLE 1. The objective results of defogging images of Figure.7.

Method	Fish			Traffic			Road			Airport		
	AG	*IE*	*EG*	*AG*	*IE*	*EG*	*AG*	*IE*	*EG*	*AG*	*IE*	*EG*
Original image	1.48	6.91	15.52	1.43	6.26	15.17	4.66	7.29	47.83	5.49	6.80	55.59
SSR	2.53	7.20	26.32	2.95	7.13	30.72	4.56	6.86	46.52	7.05	6.99	70.74
MSR	2.50	7.18	26.06	2.90	7.05	30.48	4.58	6.98	46.84	7.35	7.08	74.04
MSRCR	3.97	7.23	41.53	3.86	7.10	40.73	5.74	7.07	58.82	11.78	7.58	119.00
He	2.00	7.31	20.94	3.90	7.15	41.30	5.23	7.27	53.36	9.72	7.50	98.40
Wang	4.36	7.53	45.29	4.36	7.35	45.34	6.28	7.18	63.96	13.08	7.73	131.17
Cai	1.95	7.11	20.58	2.89	7.00	30.23	5.62	7.44	57.83	7.38	7.31	74.30
Zhu	1.46	6.64	15.27	2.80	7.00	29.23	5.12	7.28	52.67	8.32	7.22	83.82
Meng	3.924	7.52	41.46	6.97	7.16	73.42	7.00	7.32	71.08	16.39	7.59	165.92
Our	**7.19**	**7.80**	**73.40**	**8.04**	**7.60**	**82.13**	**11.13**	**7.33**	**111.39**	**22.14**	**7.88**	**216.79**

The *AG* is expressed by:

$$AG = \frac{1}{(M-1)(N-1)} \sum_{i=1}^{M-1} \times \sum_{j=1}^{N-1} \sqrt{\frac{(f(i+1,j)-f(i,j))^2+(f(i,j+1)-f(i,j))^2)}{2}} \tag{36}$$

where f is the input image, and M is the width of f, N is the height of f. *AG* reflects the change of the detail information. It represents the rate of density change of the image in multi-dimensional direction, which represents clarity of the defogged image. The defogged image has more clarity when the *AG* value is larger.

The *IE* is described as:

$$IE = -\sum_{i=0}^{n} p_i log_2 p_i \tag{37}$$

where n is the total number of grayscale level, i is the pixel value, p_i is the probability of occurrence of a pixel value which is determined by the ratio of the number of a pixel value i to the total number of pixels. The *IE* is the average information of the image, which is used to describe the pixel distribution and aggregation features of the image. The larger of the *IE* value represents that the color information of the images is richer.

EG reflects the changes of edge gradient. The *EG* represents a significant level of change in pixel value near the pixel of the step change. The larger of the *EG* value, the better of the edge retention capability. We define *EG* as:

$$EG = \frac{\sum_{i=1}^{n} |E_1 - E_2|_{enhancement}}{\sum_{i=1}^{n} |E_1 - E_2|_{original}} \tag{38}$$

where n is the total number of the pixels in the image, E_1 is the pixel value of adjacent cells, the same to E_2.

2) EVALUATION RESULTS AND ANALYSIS

In order to avoid inequity in subjective visual Metrics, objective and fair analysis of different evaluation methods are needed. Therefore, an objective analysis is adopted to evaluate the image effect of the selected algorithm. The average gradient, information entropy, and edge intensity of Figure. 7 are shown according to formula (36), (37), and (38), respectively. All experimental results are recorded in Table 1.

In term of the data analysis of Table 1., we compare the three objective metrics values of the defogged image processed by SSR, MSR, MSRCR, He *et al*. [20], Wang *et al*. [10], Cai *et al*. [21], Meng *et al*. [50], and our algorithm. Our method is superior to the original image from the objective metrics and subjective analysis. It indicates that details and contrast of the images can be greatly extent improved by our method. The Fig.7-fish(h) is enhanced by Zhu *et al*. [49]. The *AG* and *IE* are barely inferior to the original image in Figure.7-fish (a). Therefore, Zhu *et al*. [49] are not suitable for applying to underwater images.

As we can see, the algorithms of Zhu *et al.* [49] and Cai *et al.* [21] perform poorly, the results with halo artifacts and color distortion. The richness of image detail information determines the *IE* value. The *IE* values of two methods are lower than another state-of-the-art. He *et al.* [20] and Meng *et al.* [50] can enhance image contrast but over-enhancement. Some quantitative metrics are inferior to Wang *et al.* [10]. The LP_MSRCR based on MSRCR is proposed for the purpose of obtaining the enhanced images with clearer and higher contrast. As a whole, our method outperforms other classical and state-of-the-art algorithms in three objective metrics. The experimental results demonstrate the effectiveness of our method can be applied to image defogging.

IV. CONCLUSION

We proposed a retinex-based laplacian pyramid method for image defogging, which combines the advantages of multi-scale convolution and laplacian pyramid detail enhancement. We extract the detail information by multi-scale convolution

and use the improved laplacian pyramid to enhance the edge detail of the image. In order to avoid over-enhancement since the illumination is directly removed, we add the corrected illumination back to the reflection component as a complementary process, which has better natural performance. From the subjective and objective evaluation, the method effectively enhances the edge detail information and preserves the color consistency of the image. We provide a novel solution for image defogging, but there are some places need to be improved. On the one hand, most of the parameters are set empirically, which can be applied to image defogging of some scenes. However, since some parameters cannot be adaptively adjusted, satisfactory defogging effects cannot be guaranteed. On the other hand, the complexity of calculating will be higher due to uses multi-scale gaussian convolution and bilateral filter. We will research these issues in future work.

REFERENCES

[1] R. T. Tan, "Visibility in bad weather from a single image," in *Proc. IEEE Conf. Comput. Vis. Pattern Recognit.*, Jun. 2008, pp. 1–8.
[2] R. Fattal, "Single image dehazing," *ACM Trans. Graph.*, vol. 27, no. 3, pp. 1–9, 2008.
[3] S.-Y. Yu and H. Zhu, "Low-illumination image enhancement algorithm based on a physical lighting model," *IEEE Trans. Circuits Syst. Video Technol.*, vol. 29, no. 1, pp. 28–37, Jan. 2019.
[4] Y. Guo, X. Ke, J. Ma, and J. Zhang, "A pipeline neural network for low-light image enhancement," *IEEE Access*, vol. 7, pp. 13737–13744, 2019.
[5] W. Kim, "Image enhancement using patch-based principal energy analysis," *IEEE Access*, vol. 6, pp. 72620–72628, 2018.
[6] T. Dong, G. Zhao, J. Wu, Y. Ye, and Y. Shen, "Efficient traffic video dehazing using adaptive dark channel prior and spatial–temporal correlations," *Sensors*, vol. 19, Apr. 2019.
[7] K. Pyka, "Wavelet-based local contrast enhancement for satellite, aerial and close range images," *Remote Sens.*, vol. 9, no. 1, Jan. 2017.
[8] Y. Zhou, Q. Wu, K. Yan, L. Feng, and W. Xiang, "Underwater image restoration using color-line model," *IEEE Trans. Circuits Syst. Video Technol.*, vol. 29, no. 3, pp. 907–911, Mar. 2019.
[9] X. Pan, D. Yang, L. Li, Z. Liu, H. Yang, Z. Cao, Y. He, Z. Ma, and Y. Chen, "Cell detection in pathology and microscopy images with multi-scale fully convolutional neural networks," *World Wide Web*, vol. 21, pp. 1721–1743. Nov. 2018.
[10] J. Wang, K. Lu, J. Xue, N. He, and L. Shao, "Single image dehazing based on the physical model and MSRCR algorithm," *IEEE Trans. Circuits Syst. Video Technol.*, vol. 28, no. 9, pp. 289–292, Sep. 2018.
[11] Y. Liu, J. Shang, L. Pan, A. Wang, and M. Wang, "A unified variational model for single image dehazing," *IEEE Access*, vol. 7, pp. 15722–15736, 2019.
[12] M. Ju, Z. Gu, and D. Zhang, "Single image haze removal based on the improved atmospheric scattering model," *Neurocomputing*, vol. 260, pp. 180–191, Oct. 2017.
[13] S. K. Nayar and S. G. Narasimhan, "Vision in bad weather," in *Proc. 7th Int. Conf. Comput. Vis.*, 1999, pp. 820–827.
[14] S. G. Narasimhan and S. K. Nayar, "Vision and the atmosphere," *Int. J. Comput. Vis.*, vol. 48, no. 3, pp. 233–254, 2002.
[15] W. Wang, F. Chang, T. Ji, and X. Wu, "A fast single-image dehazing method based on a physical model and gray projection," *IEEE Access*, vol. 6, pp. 5641–5653, 2018.
[16] Y. Y. Schechner, S. G. Narasimhan, and S. K. Nayar, "Instant dehazing of images using polarization," in *Proc. IEEE Conf. Comput. Vis. Pattern Recognit.*, vol. 1, Dec. 2001, pp. 325–332.
[17] S. G. Narasimhan and S. K. Nayar, "Interactive (de) weathering of an image using physical models," in *Proc. 7th Int. Conf. Comput. Vis.*, Oct. 2003, pp. 820–827.
[18] X. Dong, G. Wang, Y. Pang, W. Li, J. Wen, W. Meng, and Y. Lu, "Fast efficient algorithm for enhancement of low lighting video," in *Proc. IEEE Int. Conf. Multimedia Expo (ICME)*, Jul. 2011, pp. 1–6.
[19] K. Nishino, L. Kratz, and S. Lombardi, "Bayesian defogging," *Int. J. Comput. Vis.*, vol. 98, no. 3, pp. 263–278, Jul. 2012.
[20] K. He, J. Sun, and X. Tang, "Single image haze removal using dark channel prior," *IEEE Trans. Pattern Anal. Mach. Intell.*, vol. 33, no. 12, pp. 2341–2353, Dec. 2011.
[21] B. Cai, X. Xu, K. Jia, C. Qing, and D. Tao, "DehazeNet: An end-to-end system for single image haze removal," *IEEE Trans. Image Process.*, vol. 25, no. 11, pp. 5187–5198, Nov. 2016.
[22] H. Zhang and V. M. Patel, "Densely connected pyramid dehazing network," in *Proc. CVPR*, Jun. 2018, pp. 3194–3203.
[23] X. Yang, Z. Xu, and J. Luo, "Towards perceptual image dehazing by physics-based disentanglement and adversarial training," in *Proc. 32nd AAAI Conf. Artif. Intell.*, Apr. 2018, pp. 1–8.
[24] B. Li, X. Peng, Z. Wang, J. Xu, and D. Feng, "Aod-Net: All-in-one dehazing network," in *Proc. IEEE Int. Conf. Comput. Vis. (ICCV)*, Oct. 2017, pp. 4770–4778.
[25] D. Chen, M. He, Q. Fan, J. Liao, L. Zhang, D. Hou, and G. Hua, "Gated context aggregation network for image dehazing and deraining," in *Proc. IEEE Winter Conf. Appl. Comput. Vis.*, Jan. 2019, pp. 1375–1383.
[26] W. Ren, L. Ma, J. Zhang, J. Pan, X. Cao, W. Liu, and M.-H. Yang, "Gated fusion network for single image dehazing," in *Proc. CVPR*, Mar. 2018, pp. 3253–3261.
[27] D. Engin, A. Genç, and H. K. Ekenel, "Cycle-dehaze: Enhanced cyclegan for single image dehazing," in *Proc. CVPR*, May 2018, pp. 825–833.
[28] C. Y. Wong, G. Jiang, M. A. Rahman, S. Liu, S. C.-F. Lin, N. Kwok, H. Shi, Y.-H. Yu, and T. Wu, "Histogram equalization and optimal profile compression based approach for colour image enhancement," *J. Vis. Commun. Image Represent.*, vol. 38, pp. 802–813, Jul. 2016.
[29] Y. Fei and F. Shao, "Contrast adjustment based on image retrieval," *Laser Optoelectron. Progress.*, vol. 55, Nov. 2017.
[30] V. Magudeeswaran and J. F. Singh, "Contrast limited fuzzy adaptive histogram equalization for enhancement of brain images," *Int. J. Imag. Syst. Tech.*, vol. 27, pp. 98–103, Mar. 2017.
[31] H. Hiary, R. Zaghloul, A. Al-Adwan, and M. Al-Zoubi, "Image contrast enhancement using geometric mean filter," *Single, Image Video Process.*, vol. 11, pp. 833–840, Jul. 2017.
[32] G. Wanga, D. Li, W. Pan, and Z. Zang, "Modified switching median filter for impulse noise removal," *Signal Process.*, vol. 90, no. 12, pp. 3213–3218, Dec. 2010.
[33] L. Xiao, C. Li, Z. Wu, and T. Wang, "An enhancement method for X-ray image via fuzzy noise removal and homomorphic filtering," *Neurocomputing*, vol. 195, pp. 56–64, Jun. 2016.
[34] C. Tomasi and R. Manduchi, "Bilateral filtering for gray and color images," in *Proc. 6th IEEE Int. Conf. Comput. Vis.*, Jan. 1998, pp. 839–846.
[35] M. A. Hussain, A. Sheikh-Akbari, and E. A. Halpin, "Color constancy for uniform and non-uniform illuminant using image texture," *IEEE Access*, vol. 7, pp. 72964–72978, 2019.
[36] D. J. Jobson, Z.-U. Rahman, and G. A. Woodell, "Properties and performance of a center/surround Retinex," *IEEE Trans. Image Process.*, vol. 6, no. 3, pp. 451–462, Mar. 1997.
[37] X. Liu, D. Zhai, R. Chen, X. Ji, D. Zhao, and W. Gao, "Depth super-resolution via joint color-guided internal and external regularizations," *IEEE Trans. Image Process.*, vol. 28, no. 4, pp. 1636–1645, Apr. 2019.
[38] H.-M. Hu, Q. Guo, J. Zheng, H. Wang, and B. Li, "Single image defogging based on illumination decomposition for visual maritime surveillance," *IEEE Trans. Image Process.*, vol. 28, no. 6, pp. 2882–2897, Jun. 2019.
[39] M. Elad, "Retinex by two bilateral filters," in *Scale Space and PDE Methods in Computer Vision*, 2005, pp. 7–10.
[40] Y. Liu, H. Yan, S. Gao, and K. Yang, "Criteria to evaluate the fidelity of image enhancement by MSRCR," *IET Image Process.*, vol. 12, pp. 880–887, May 2018.
[41] J. Shen, Y. Zhao, S. Yan, and X. Li, "Exposure fusion using boosting Laplacian pyramid," *IEEE Trans. Cybern.*, vol. 44, no. 9, pp. 1579–1590, Sep. 2014.
[42] L. Huang, G. Cao, and L. Yu, "Efficient contrast enhancement with truncated adaptive gamma correction," in *Proc. 9th Int. Congr. Image Signal Process., BioMed. Eng. Inform.*, Oct. 2016, pp. 189–194.
[43] R. Kimmel, M. Elad, D. Shaked, R. Keshet, and I. Sobel, "A variational framework for retinex," *Int. J. Comput. Vis.*, vol. 52, no. 1, pp. 7–23, Apr. 2003.
[44] X. Fu, D. Zeng, Y. Huang, X.-P. Zhang, and X. Ding, "A weighted variational model for simultaneous reflectance and illumination estimation," in *Proc. CVPR*, Jun. 2016, pp. 2782–2790.

[45] P. J. Burt and E. H. Adelson, "The Laplacian pyramid as a compact image code," *IEEE Trans. Commun.*, vol. COM-31, no. 4, pp. 532–540, Apr. 1983.
[46] W. Zhang, L. Dong, X. Pan, J. Zhou, L. Qin, and W. Xu, "Single image defogging based on multi-channel convolutional MSRCR," *IEEE Access*, vol. 7, pp. 72492–72504, 2019.
[47] A. B. Petro, C. Sbert, and J.-M. Morel, "Multiscale retinex," *Image Process. Line*, vol. 4, pp. 71–88, Apr. 2014.
[48] K. He, J. Sun, and X. Tang, "Guided image filtering," *IEEE Trans. Pattern Anal. Mach. Intell.*, vol. 35, no. 6, pp. 1397–1409, Jun. 2013.
[49] Q. Zhu, J. Mai, and L. Shao, "A fast single image haze removal algorithm using color attenuation prior," *IEEE Trans. Image Process.*, vol. 24, no. 11, pp. 3522–3533, Nov. 2015.
[50] G. Meng, Y. Wang, J. Duan, S. Xiang, and C. Pan, "Efficient image dehazing with boundary constraint and contextual regularization," in *Proc. IEEE Int. Conf. Comput. Vis. (ICCV)*, Dec. 2013, pp. 617–624.
[51] N. He, J.-B. Wang, L.-L. Zhang, and K. Lu, "An improved fractional-order differentiation model for image denoising," *Signal Process.*, vol. 112, pp. 180–188, Sep. 2015.
[52] Y. Chen, Z. Li, B. Bhanu, D. Tang, Q. Peng, and Q. Zhang, "Improve transmission by designing filters for image dehazing," in *Proc. IEEE 3rd Int. Conf. Image, Vis. Comput. (ICIVC)*, Jun. 2018, pp. 274–378.

JINGCHUN ZHOU received the B.S. degree in computer science and technology from the Daqing Normal College, Daqing, China, in 2012, and the M.S. degree in software engineering from the Beijing University of Posts and Telecommunications, Beijing, China, in 2016. He is currently pursuing the Ph.D. degree in computer application with the Dalian Maritime University, Dalian, China. His research interests include image enhancement and fusion. He is also a Journal Reviewer of IEEE Access.

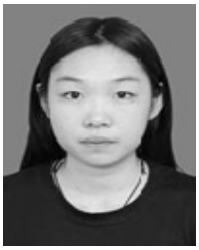

DEHUAN ZHANG received the B.S. degree in software engineering from Henan Polytechnic University, Jiaozuo, China, in 2018. She is currently pursuing the M.S. degree with Dalian Maritime University. Her research interests include image processing, image enhancement, and target detection.

PEIYU ZOU received the B.S. degree in software engineering and Japanese from Dalian Jiao Tong University, Dalian, China, in 2018. He is currently pursuing the M.S. degree with Dalian Maritime University. His main research interests include image processing, image enhancement, and target recognition.

WEIDONG ZHANG received the B.S. degree in computer science and technology from the Xinke College of Henan Institute of Science and Technology, Xinxiang, China, in 2015, and the M.S. degree in computer science and technology from the Guilin University of Electronic Technology, Guilin, China, in 2018. He is currently pursuing the Ph.D. degree in information and communication engineering with Dalian Maritime University, Dalian, China. He has authored (coauthored) five research articles. His main research interests include image enhancement and defogging, and target recognition. He is also a Journal Reviewer of IEEE Access.

WEISHI ZHANG was born in Liaoning, China. He received the B.S. degree in computer science from Xi'an Jiaotong University, China, in 1984, the M.S. degree in computer science from the Chinese Academy of Sciences, China, in 1986, and the Ph.D. degree in computer science from the University of Munich, Germany, in 1996. From 1986 to 1990, he was an Assistant Researcher with the Shenyang Institute of Computing, Chinese Academy of Sciences, China. From 1990 to 1992, he was a Visiting Scholar with Passau University, Germany. From 1992 to 1997, he was an Assistant Professor with the University of Munich, Germany. In 1997, he joined the Department of Computer Science, Dalian Maritime University, China, where he is currently a Full Professor with the School of Information Science and Technology. His research interests include big data intelligent processing, software engineering, software architecture, formal specification techniques, and program semantics model.